J|A|C|S COMMUNICATIONS

Published on Web 09/02/2009

Thiolate-Protected $Au_{20}(SR)_{16}$ Cluster: Prolate Au_8 Core with New $[Au_3(SR)_4]$ Staple Motif

Yong Pei, Yi Gao, Nan Shao, and Xiao Cheng Zeng*

Department of Chemistry and Nebraska Center for Materials and Nanoscience, University of Nebraska-Lincoln, Lincoln, Nebraska 68588

Received June 30, 2009; E-mail: xczeng@phase2.unl.edu

It is well-established that gold nanoclusters possess remarkable catalytic activities.[1] However, the structure−activity relationship of gold nanoclusters is largely an open question due in part to the lack of precise atomic structures of gold clusters. To date, gold clusters reported in the literature can be loosely divided into two classes: bare gold clusters (Au_N) and ligand-stabilized gold clusters. Bare gold anion clusters in the size range $2 \le N \le 20$, which have been well-studied, undergo a series of structural transitions from planar to flat shell to cage to pyramid.[2] For medium-sized gold clusters beyond Au_{24}, the compact core/shell structures are likely a prevalent structural form.[3] On the other hand, ligand-stabilized gold clusters typically exhibit structural patterns different from those of bare clusters. A unique structural feature in many ligand-protected Au_N (LP-Au_N) clusters is the existence of a symmetric Au core. Previous experimental and theoretical studies have revealed several forms of symmetric Au cores, e.g., the incomplete icosahedrons Au_8, Au_9, Au_{10}, and Au_{11}, the perfect icosahedron Au_{13}, and hexagonally packed Au_{39}, in various phosphine−X (X = Cl, SCN, etc.)-protected gold salts.[4] Monodisperse $Au_{55}(PPh_3)_{12}Cl_6$ clusters synthesized in the laboratory had been proposed to contain either a cuboctahedral or an icosahedral Au_{55} core.[4] The recent crystallization of the thiolate-protected gold cluster $Au_{102}(p\text{-MBA})_{44}$ (*p*-MBA = $SC_7O_2H_5$) was a major advance.[5a] The Au core of this nanocluster was found to be highly symmetric, protected by two types of "staple" motifs, namely, the simple motif −RS−Au−RS− and the extended motif −RS−Au−RS−Au−RS−.[5] A similar Au core/staple motif combination was also discovered in the thiolate-protected gold cluster $Au_{25}(SR)_{18}^-$, which possesses an icosahedral Au_{13} core and six −RS−Au−RS−Au−RS− extended staple motifs.[6] Besides $Au_{102}(SR)_{44}$ and $Au_{25}(SR)_{18}^-$, the presence of several size-selected clusters (e.g., 5, 8, 14, 22, and 28 kDa Au species) was revealed by mass spectrometry.[7,8] However, the crystallization and identification of the structural formula of these clusters are rather difficult. The 5, 8, 14, and 28 kDa Au species had been assigned to $Au_{25}(SR)_{18}$, $Au_{38}(SR)_{24}$, $Au_{68}(SR)_{34}$, and $Au_{144}(SR)_{59}$, respectively.[7,8] Recently, the Au core and associated staple motifs of $Au_{12}(SR)_9^+$,[9a] $Au_{38}(SR)_{24}$,[9b,10] and $Au_{144}(SR)_{60}$[11] have been predicted theoretically. In addition, a structural formulation of $[Au]_{19+30}[Au(SR)_2]_{11}[Au_2(SR)_3]_4$ was predicted for the 14 kDa cluster $Au_{68}(SR)_{34}$.[12] Intriguing core−ligand combinations in these highly stable LP-Au_N clusters were partially attributed to the closed valence-electron shell.[5,6,10]

In this communication, we present a theoretical prediction of the most viable structure of the newly synthesized "magic cluster" $Au_{20}(SR)_{16}$ (R = CH_2CH_2Ph).[13] A related finding is the possible existence of a new type of extended staple motif, namely, −RS−Au−RS−Au−RS−Au−RS−. The recent experiment shows that $Au_{20}(SR)_{16}$ exhibits robust stability toward excess thiol etching and has a large optical absorption gap (∼2.15 eV).[13] In fact, the number of core Au atoms and thiolate ligands in $Au_{20}(SR)_{16}$ exhibits a good linear correlation with those known core sizes, for example, 25-, 38-, 68-, 102-, and 144-atom clusters (Figure S1 in the Supporting Information). Our structural prediction is based on the "divide-and-protect" scheme, that is, any stable thiolate-protected gold cluster $Au_N(SR)_i$ can be viewed as a Au core plus a number of level-*m* staple motifs, e.g., $[Au]_{a+a'}[Au(SR)_2]_b[Au_2(SR)_3]_c$.[10,14] Here we define a level-*m* staple motif $[Au_m(SR)_{m+1}]$ according to the number of Au atoms in the motif. To date, only level-1 and level-2 staple motifs have been observed in $Au_N(SR)_i$ clusters.[5,6,9−11] Higher-level staple motifs, such as the level-3 staple motif, have been seen only in certain high-energy isomers of the $Au_{38}(SR)_{24}$ cluster.[15]

On basis of well-established cluster structures from both experiment and theory, we have identified a generic rule: *higher-level staple motifs become more prevalent as the Au/SR ratio in a cluster decreases*. For example, the ratio of level-1 to level-2 staple motifs is 30:0, 19:2, 11:4, 3:6, and 0:6 in $Au_{144}(SR)_{60}$, $Au_{102}(SR)_{44}$, $Au_{68}(SR)_{34}$, $Au_{38}(SR)_{24}$, and $Au_{25}(SR)_{18}$, respectively. The homoleptic $[Au(SR)]_N$ clusters have a Au/SR ratio of 1:1. The existence of higher-level staple motifs (e.g., level-3, level-4, etc.) in the homoleptic $[Au(SR)]_N$ clusters are plausible on the basis of various Au core/staple motif partitions, for example, $Au_{N/2}[Au(SR)_2]_{N/2}$, $Au_{N/3}[Au_2(SR)_3]_{N/3}$, $Au_{N/4}[Au_3(SR)_4]_{N/4}$, etc. However, the homoleptic $[Au(SR)]_N$ species has no stacked Au core but exhibits only chain, ring, and catenane structures, depending on *N*.[16] $Au_{20}(SR)_{16}$ has a Au/SR ratio of 1.25:1, a value between that of the core-free $[Au(SR)]_N$ and core-stacked structures [e.g., 1.39:1 for $Au_{25}(SR)_{18}$]. In view of the low Au/SR ratio in $Au_{20}(SR)_{16}$, the level-3 extended staple motif was added in the structural formula, i.e., $[Au]_{a+a'}[Au(SR)_2]_b[Au_2(SR)_3]_c[Au_3(SR)_4]_d$, with several constraints: $a' = 2b + 2c + 2d$, $a' + a + b + 2c + 3d = 20$, and $2b + 3c + 4d = 16$. A unique set of data, $a = 0$, $a' = 8$, $b = 0$, $c = 0$, and $d = 4$, satisfy *all constraints* in the division scheme (Table S1 in the Supporting Information). On the basis of this set, a number of isomer structures were built and optimized using density functional theory (DFT).[17] Here, the −R group is simplified to a methyl ($-CH_3$) group for computing efficiency. In addition, isomers built upon a highly stable tetrahedral Au_{20} core were investigated by randomly adding 16 $-SCH_3$ groups. Finally, global-minimum search techniques such as the basin-hopping algorithm[18] and simulated annealing were also applied to explore various isomer structures. Altogether, more than 50 isomer structures were optimized using the generalized gradient approximation with the Perdew−Burke−Ernzerhof (PBE) functional[19a] and the double-ζ basis set (DND), as implemented in the DMol^3 software package.[19b] The 10 lowest-lying isomer structures ranked at the PBE/DND level were reoptimized at the PBE/TZP level of theory followed by single-point energy calculations including spin−orbit effects, using the ADF software package.[20] Lastly, for the three lowest-energy isomers ranked at the PBE/TZP level (**Iso1**−**Iso3**), structural

10.1021/ja905359b CCC: $40.75

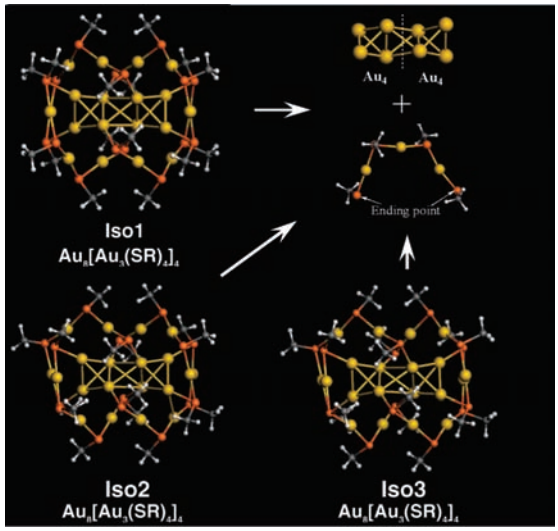

Figure 1. Structures of **Iso1**−**Iso3** and structural decomposition of the Au_8 core and four level-3 staple motifs. Structures of isomers **Iso4**−**Iso6** are shown in Figure S1.

Table 1. Relative Electronic Energies and Gibbs Free Energies and Lowest Vibrational Frequencies of **Iso1**−**Iso3** (Energies Are in eV)

isomer	PBE/TZP	PBE/LANL2DZ,6-31G(d,p)	TPSS/LANL2DZ,6-31G(d,p)
Iso1	0.00/0.00[a]	0.00/0.00[b]	0.00/0.00[b]
Iso2	0.022/0.026[a]	0.012/−0.12[b]	0.002/0.11[b]
Iso3	0.041/0.052[a]	0.078/−0.075[b]	0.063/0.083[b]

[a] Including spin−orbit effects. [b] Gibbs free energy at 300 K.

optimizations, frequency calculations, and Gibbs free energy corrections at 300 K were carried out using the PBE and TPSS[21a] functionals, respectively, with the LANL2DZ basis set for Au and the 6-31G(d,p) basis set for S, C, and H, as implemented in the Gaussian 03 program package.[21b]

As shown in Figure 1, the three lowest-lying structures **Iso1**−**Iso3** obtained all indicate that $Au_{20}(SCH_3)_{16}$ consists of a *prolate*-shaped Au_8 core and four level-3 $[Au_3(SR)_4]$ staple motifs. **Iso1**−**Iso3** are also local-minimum structures, as confirmed by frequency calculations, with the same $[Au]_8[Au_3(SR)_4]_4$ structural division but slightly different orientations of the staple motifs and Au−Au bond lengths in the Au-core. Moreover, independent DFT calculations using two different functionals and three different basis sets with and without inclusion of spin−orbit effects all show that the three isomers **Iso1**−**Iso3** are nearly degenerate in energy (Table 1). In addition, the computed relative Gibbs free energies of **Iso1**−**Iso3** at 300 K suggest that the three isomers may coexist at room temperature. Other isomers with different Au cores or staple motifs all have notably higher energies [>0.40 eV at the TPSS/LANL2DZ,6-31G(d,p) level] than **Iso1**−**Iso3** and also give significantly different optical absorption curves (see below). Despite the high stability of tetrahedral Au_{20}, we found that the addition of 16 $-SCH_3$ ligands to this species leads to significant distortion of the tetrahedral structure. As a result, the thiolate-covered tetrahedral Au_{20} clusters have much higher energies (>1.6 eV) than **Iso1**−**Iso3**.

The Au_8 cores in **Iso1**−**Iso3** have near-D_{2d} symmetry. Bond length analysis indicates that the Au_8 core can be viewed as two edge-fused tetrahedral Au_4 units (Figure 1), as the Au−Au bond lengths between the two Au_4 units (3.0−3.4 Å) are much longer than those (2.7−2.9 Å) within a single Au_4 unit. Each Au atom in the Au_8 core is protected by an ending point of the level-3 staple motif. The arrangement of staple motifs in **Iso1**−**Iso3** is quite

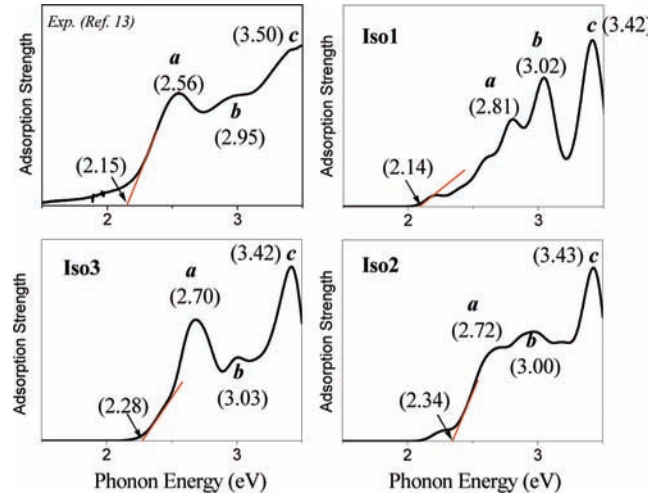

Figure 2. Comparison of experimental and theoretical optical absorption spectra of **Iso1**−**Iso3** of $Au_{20}(SR)_{16}$. **Iso1**−**Iso3** have the same prolate Au core.

unique in that the two ending points of a level-3 staple motif connect with two Au atoms in different Au_4 units. Such an arrangement of staple motifs further enhances the stability of the prolate Au core. Notably, the unprotected prolate Au_8 cluster itself is not a local-minimum structure. In fact, geometry optimization of prolate Au_8 leads to a planar structure.

The optical absorption spectrum of a thiolate-protected gold cluster can be very sensitive to the core structure,[10] and this can be exploited to differentiate structures of different isomers. Here the optical absorption spectra of six isomers, **Iso1**−**Iso6**, were computed by the time-dependent DFT (TD-DFT) method at the PBE/TZP level using the ADF software package. Figure 2 shows that the extrapolated optical band edges of **Iso1**−**Iso3** are 2.14, 2.34, and 2.28 eV, respectively, in good agreement with the experimental band edge of 2.15 eV. Moreover, three prominent absorption peaks, ***a*** (2.56 eV), ***b*** (2.95 eV), and ***c*** (3.50 eV), in the experimental absorption curve are well-reproduced by the theoretical spectra of **Iso1**−**Iso3** (Figure 2). In particular, the theoretical optical absorption spectrum of **Iso3** is in the best agreement with the experimental one. The different shapes of the simulated absorption curves of **Iso1**−**Iso3** are mainly due to slightly different geometries of the staple motifs and Au−Au bond lengths in the Au-core structure (Figure 1), reaffirming the sensitivity of the optical absorption spectrum to the Au core structure. The optical absorption spectra of the higher-energy isomers (**Iso4**−**Iso6**) are significantly different from those of **Iso1**−**Iso3** (Figure S1). The optical gaps for **Iso4**−**Iso6** are 1.3−1.7 eV, much less than the experimental gap of 2.15 eV.

Further examination of the Kohn−Sham (KS) molecular orbital (MO) energy levels and the atomic orbital components in each KS MO of **Iso1**−**Iso3** indicates that the Au_8 core contributes mainly to the three strong absorption peaks (***a***−***c***) in the optical spectrum. Figure 3 represents the KS orbital energies and components of **Iso1** (KS orbital energies and components of **Iso2** and **Iso3** are given in Figure S3). As shown in Figure 3, the unoccupied LUMO to LUMO+5 are mainly composed of the Au(6sp) orbital, denoted as the sp band. The set of occupied orbitals HOMO-28 to HOMO are d band because of the significant contribution of Au(5d) atomic orbitals.

The X-ray diffraction (XRD) patterns of **Iso1**−**Iso6** were also simulated and are shown in Figure S4. **Iso1**−**Iso3** with the same prolate Au core exhibit a single strongest peak at ∼3.8 nm^{-1}. In

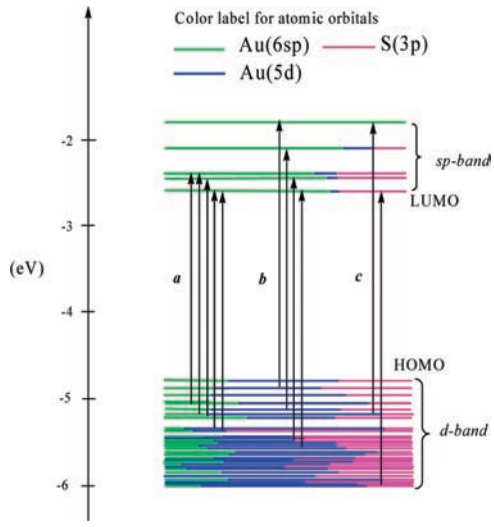

Figure 3. KS orbital energy level diagram for **Iso1**, with the three peaks **a**, **b**, and **c** in Figure 2 assigned to various excitation modes. The energies are in eV. Various colors are used to mark relative contributions (line length with color labels) of different atomic orbitals. The major orbital contributions, i.e., those from the Au(6sp), Au(5d), and S(3p) atomic orbitals, are in green, blue, and yellow, respectively. Figure 3 as drawn partially refers to ref 6c.

contrast, two peaks can be seen in the range 1.8−6.0 nm^{-1} for **Iso4**−**Iso6**. This result confirms the uniqueness of the prolate-shaped Au_8 core.

The predicted prolate Au core structure may be understood on the basis of a nonspherical shell model (e.g., the Clemenger−Nilsson model[22]). According to the electronic shell model,[5d] $Au_{20}(SR)_{16}$ has four net free valence electrons (20 − 16 = 4) from Au atoms. In the Clemenger−Nilsson model,[22] the disorder parameter (η) of a nonspherical metal cluster is defined as $\eta = 2(R_x - R_z)/(R_x + R_z)$, where R_x and R_z are the length and diameter, respectively, of a prolate-shaped cluster. Here η is estimated to be 0.78 on the basis of the Au core structure of **Iso1**, in good agreement with the value of 0.7 predicted from the Clemenger−Nilsson model[22a] for an alkali metal cluster with four valence electrons.

In summary, we have shown that the recently synthesized $Au_{20}(SR)_{16}$ cluster contains a *prolate* Au_8 core and four level-3 extended staple motifs −RS−Au−RS−Au−RS−Au−RS−. This highly stable cluster may represent a structural evolution of thiolate-protected gold clusters from the homoleptic core-free structure to the core-stacked structure. The predicted Au-core/ligand structure is supported by very good agreement between the theoretical and experimental optical absorption spectra and by the identification of the structure as the best candidate for the lowest-energy structure through an extensive structural search.

Acknowledgment. We thank Professor Rongchao Jin for helpful discussions and sending the original optical absorption data. This work was supported by NSF (CHE-0427746, DMR-0820521), the Nebraska Research Initiative, and the University of Nebraska Holland Computing Center.

Supporting Information Available: Computational details, isomer structures, optical spectra, coordinates, and simulated XRD patterns of various isomers. This material is available free of charge via the Internet at http://pubs.acs.org.

References

(1) (a) Haruta, M. *Catal. Today* **1997**, *36*, 153. (b) Chen, M. S.; Goodman, D. W. *Science* **2004**, *306*, 252. (c) Hughes, M. D.; Xu, Y.; Jenkins, P.; McMorn, P.; Landon, P.; Enache, D. I.; Carley, A. F.; Attard, G. A.; Hutchings, G. J.; King, F.; Stitt, E. H.; Johnston, P.; Griffin, K.; Kiely, C. J. *Nature* **2005**, *437*, 1132. (d) Yoon, B.; Häkkinen, H.; Landman, U.; Wörz, A. S.; Antonietti, J.-M.; Abbet, S.; Judai, K.; Heiz, U. *Science* **2005**, *307*, 403. (e) Turner, M.; Golvoko, V. B.; Vaughan, O. P. H.; Abdulkin, P.; Berenguer-Murcia, A.; Tikhov, M. S.; Johnson, B. F. G.; Lambert, R. M. *Nature* **2008**, *454*, 981. (f) Herzing, A. A.; Kiely, C. J.; Carley, A. F.; Landon, P.; Hutchings, G. J. *Science* **2008**, *321*, 1331.

(2) (a) Furche, F.; Ahlrichs, R.; Weis, P.; Jacob, C.; Gilb, S.; Bierweiler, T.; Kappes, M. M. *J. Chem. Phys.* **2002**, *117*, 6982. (b) Häkkinen, H.; Yoon, B.; Landman, U.; Li, X.; Zhai, H. J.; Wang, L. S. *J. Phys. Chem. A* **2003**, *107*, 6168. (c) Li, J.; Li, X.; Zhai, H. J.; Wang, L. S. *Science* **2003**, *299*, 864. (d) Bulusu, S.; Li, X.; Wang, L. S.; Zeng, X. C. *Proc. Natl. Acad. Sci. U.S.A.* **2006**, *103*, 8326. (e) Xing, X.; Yoon, B.; Landman, U.; Parks, J. H. *Phys. Rev. B* **2006**, *74*, 165423. (f) Johansson, M. P.; Lechtken, A.; Schooss, D.; Kappes, M. M.; Furche, F. *Phys. Rev. A* **2008**, *77*, 053202. (g) Lechtken, A.; Neiss, C.; Kappes, M. M.; Schooss, D. *Phys. Chem. Chem. Phys.* **2009**, *11*, 4344. (h) Huang, W.; Wang, L. S. *Phys. Rev. Lett.* **2009**, *102*, 153401. (i) Huang, W.; Bulusu, S.; Pal, R.; Zeng, X. C.; Wang, L. S. *ACS Nano* **2009**, *3*, 1225. (j) Ferrighi, L.; Hammer, B.; Madsen, G. K. H. *J. Am. Chem. Soc.* **2009**, *131*, 10605. (k) Mantina, M.; Valero, R.; Truhlar, D. G. *J. Chem. Phys.* **2009**, *131*, 064706.

(3) (a) Ji, M.; Gu, X.; Li, X.; Gong, X.; Li, J.; Wang, L.-S. *Angew. Chem., Int. Ed.* **2005**, *44*, 7119. (b) Lechtken, A.; Schooss, D.; Stairs, J. R.; Blom, M. N.; Furche, F.; Morgner, N.; Kostko, O.; von Issendorff, B.; Kappes, M. M. *Angew. Chem., Int. Ed.* **2007**, *46*, 2944. (c) Bulusu, S.; Li, X.; Wang, L. S.; Zeng, X. C. *J. Phys. Chem. C* **2007**, *111*, 4790. (d) Gu, X.; Bulusu, S.; Li, X.; Zeng, X. C.; Li, J.; Gong, X. G.; Wang, L. S. *J. Phys. Chem. C* **2007**, *111*, 8228. (e) Jalbout, A. F.; Contreras-Torres, F. F.; Perez, L. A.; Garzón, I. L. *J. Phys. Chem. A* **2008**, *112*, 353.

(4) See a recent review on Au_{55} clusters and references therein: Schmid, G. *Chem. Soc. Rev.* **2008**, *37*, 1909.

(5) (a) Jadzinsky, P. D.; Calero, G.; Ackerson, C. J.; Bushnell, D. A.; Kornberg, R. D. *Science* **2007**, *318*, 430. (b) Whetten, R. L.; Price, R. C. *Science* **2007**, *318*, 407. (c) Gao, Y.; Shao, N.; Zeng, X. C. *ACS Nano* **2008**, *2*, 1497. (d) Walter, M.; Akola, J.; Lopez-Acevedo, O.; Jadzinsky, P. D.; Calero, G.; Ackerson, C. J.; Whetten, R. L.; Grönbeck, H.; Häkkinen, H. *Proc. Natl. Acad. Sci. U.S.A.* **2008**, *105*, 9157. (e) Li, Y.; Galli, G.; Gygi, F. *ACS Nano* **2008**, *2*, 1896.

(6) (a) Heaven, M. W.; Dass, A.; White, P. S.; Holt, K. M.; Murray, R. W. *J. Am. Chem. Soc.* **2008**, *130*, 3754. (b) Akola, J.; Walter, M.; Whetten, R. L.; Häkkinen, H.; Gronbeck, H. *J. Am. Chem. Soc.* **2008**, *130*, 3756. (c) Zhu, M.; Aikens, C. M.; Hollander, F. J.; Schatz, G. C.; Jin, R. *J. Am. Chem. Soc.* **2008**, *130*, 5883.

(7) (a) Schaaff, T. G.; Shafigullin, M. N.; Khoury, J. T.; Vezmar, I.; Whetten, R. L.; Cullen, W. G.; First, P. N.; Gutierréz-Wing, C.; Ascensio, J.; Jose-Yacamán, M. J. *J. Phys. Chem. B* **1997**, *101*, 7885. (b) Schaaff, T. G.; Knight, G.; Shafigullin, M. N.; Borkman, R. F.; Whetten, R. L. *J. Phys. Chem. B* **1998**, *102*, 10643. (c) Schaaff, T. G.; Shafigullin, M. N.; Khoury, J. T.; Vezmar, I.; Whetten, R. L. *J. Phys. Chem. B* **2001**, *105*, 8785.

(8) Tsunoyama, H.; Nickut, P.; Negishi, Y.; Al-Shamery, K.; Matsumoto, Y.; Tsukuda, T. *J. Phys. Chem. C* **2007**, *111*, 4153.

(9) (a) Jiang, D. E.; Whetten, R. L.; Luo, W.; Dai, S. *J. Phys. Chem. C* **2009**, in press. (b) Jiang, D. E.; Tiago, M. L.; Luo, W. D.; Dai, S. *J. Am. Chem. Soc.* **2008**, *130*, 2777.

(10) Pei, Y.; Gao, Y.; Zeng, X. C. *J. Am. Chem. Soc.* **2008**, *130*, 7830.

(11) Lopez-Acevedo, O.; Akola, J.; Whetten, R. L.; Grönbeck, H.; Häkkinen, H. *J. Phys. Chem. C* **2009**, *113*, 5035.

(12) Dass, A. *J. Am. Chem. Soc.* **2009**, *131*, 11666.

(13) Zhu, M.; Qian, H.; Jin, R. *J. Am. Chem. Soc.* **2009**, *131*, 7220.

(14) (a) Häkkinen, H.; Walter, M.; Grönbeck, H. *J. Phys. Chem. B* **2006**, *110*, 9927. (b) Chaki, N. K.; Negishi, Y.; Tsunoyama, H.; Shichibu, Y.; Tsukuda, T. *J. Am. Chem. Soc.* **2008**, *130*, 8608.

(15) Garzón, I. L.; Rovira, C.; Michaelian, K.; Beltrán, M. R.; Ordejón, P.; Junquera, J.; Sánchez-Portal, D.; Artacho, E.; Soler, J. M. *Phys. Rev. Lett.* **2000**, *85*, 5250.

(16) (a) Bau, R. *J. Am. Chem. Soc.* **1998**, *120*, 9380. (b) Bonasia, P. J.; Gindelberger, D. E.; Arnold, J. *Inorg. Chem.* **1993**, *32*, 5126. (c) Wiseman, M. R.; Marsh, P. A.; Bishop, P. T.; Brisdon, B. J.; Mahon, M. F. *J. Am. Chem. Soc.* **2000**, *122*, 12598. (d) Shao, N.; Pei, Y.; Gao, Y.; Zeng, X. C. *J. Phys. Chem. A* **2009**, *113*, 629.

(17) (a) Hohenberg, P. *Phys. Rev. B* **1964**, *136*, 864. (b) Kohn, W.; Sham, L. J. *Phys. Rev. A* **1965**, *140*, 1133.

(18) (a) Wales, D. J.; Doye, J. P. K. *J. Phys. Chem. A* **1997**, *101*, 5111. (b) Yoo, S.; Zeng, X. C. *Angew. Chem., Int. Ed.* **2005**, *44*, 1491.

(19) (a) Perdew, J. P.; Burke, K.; Ernzerhof, M. *Phys. Rev. Lett.* **1996**, *77*, 3865. (b) Delley, B. *J. Chem. Phys.* **1990**, *92*, 508. Delley, B. *J. Chem. Phys.* **2003**, *113*, 7756. DMol^3 is available from Accelrys.

(20) *ADF 2008.01*; Scientific Computing and Modelling NV: Amsterdam, 2008; http://www.scm.com.

(21) (a) Tao, J.; Perdew, J. P.; Staroverov, V. N.; Scuseria, G. E. *Phys. Rev. Lett.* **2003**, *91*, 146401. (b) Frisch, M. J.; et al. *Gaussian 03*, revision C.02; Gaussian, Inc.: Wallingford, CT, 2004.

(22) (a) Clemenger, K. *Phys. Rev. B* **1985**, *32*, 1359. (b) Nisson, S. G. K. *Dan. Vidensk. Selsk. Mat. Fys. Medd.* **1955**, *29*, 16.

JA905359B